



# Layer structure and intermolecular vibrations of water confined within graphite nanoslit

Yu-Wei Kuo, Chi-Wei Wang, Ping-Han Tang<sup>1</sup>, Ten-Ming Wu\*

*Institute of Physics, National Yang Ming Chiao-Tung University, Hsinchu 300, Taiwan*



## ARTICLE INFO

### Keywords:

Nanoconfined water  
Graphite nanoslit  
Vibrational density of states  
Instantaneous normal mode analysis

## ABSTRACT

Molecular dynamics simulations were used to study layer structure and intermolecular vibrations of water confined within graphite nanoslit. The confinement effect was investigated by varying the slit width, with water density within the geometric slit space close to that of liquid water. The vibrational density of states (DOS) of nanoconfined water was dissected with the instantaneous-normal-mode (INM) analysis. The translational INM DOS of nanoconfined water shows a linear behavior at low frequencies; however, the components parallel and perpendicular to the confining wall display different behaviors, characterized with a power-law exponent less and larger than one, respectively.

## 1. Introduction

Water confined within hydrophobic nanopores has been an attractive research topic for its significant influence on physical science, biology, and technological applications [1–3]. In the fabrication of nanodevices, water was confined within graphene slit nanopores [4], where the fabricated confinements have sharp and mechanically rigid walls and the interactions between water and the confinement are weakly van der Waals forces. It is now possible to fabricate artificial confinements with different materials [5,6] and in various geometries with sizes down to sub-nanometer (nm) scales [7,8].

Within graphene nanopores, the excluded volume effect due to the hydrophobic interactions makes confined water having higher density than liquid water, resulted in more structural ordering among water molecules or even a phase transition on structure [9,10]. Nanoconfined water forms layer structure in parallel to the confining wall [11,12] and the H-bond (HB) network is essentially different from that of bulk water [13], which is basically in tetrahedral structure. Shown by experiments, square ice was detected [14] and a small portion of water molecules interfacial to a graphene plate may have a dangling OH-group pointing to the plate [15]. By molecular dynamics (MD) simulations, where graphene nanoslit were modeled as various kinds of confining surface [16–18], the in-layer structure of nanoconfined water displays different arrangements from square and rhombic structures at high water densities to pentagonal and hexagonal structures at low water densities

### [19–21].

The layer structure of nanoconfined water gives rise to significant influence on water dynamics and even causes phenomena not happened to bulk water: As the size of graphene nanoslit was narrow down to 2 nm, a fast flow rate of nanoconfined water was observed [4] and an oscillatory behavior of shear viscosity in variation with the slit width was obtained by simulations [22]. The vibrational dynamics of water confined within hydrophobic nanopores is strongly correlated to the HB network therein. The vibrational density of states (VDOS) of water confined within carbon-based slit nanopores have been investigated by many simulation studies [12,17,23,24], with the results that molecules interfacial to a graphene sheet play a special role due to their distinct HB network but beyond the interfacial region molecules make contributions similar as bulk water because of comparable HB configurations [23]. Recently, the confinement effects on water dynamics within narrow graphene-based slit pores have been revealed by using THz spectroscopy [25], indicating that intermolecular vibrations involved in stretching and librational bands of nanoconfined water were related to its layer structure, H-bond pattern, and dangling OH-groups interfacial to graphene sheets. Also, the low-frequency VDOS of nanoconfined water is strongly influenced by the confining wall [26]. Thus, intermolecular vibrations of nanoconfined water still need to be studied.

In this paper, we used MD simulations to investigate the relation between layer structure and intermolecular vibrations of water confined within graphite nanoslit. The confinement effect was studied by

\* Corresponding author.

E-mail address: [tmw@nycu.edu.tw](mailto:tmw@nycu.edu.tw) (T.-M. Wu).

<sup>1</sup> Present address: Wafer Level Optics Organization, VisEra Technologies Company Ltd. Hsinchu Science Park, Taiwan 300778, R.O.C.

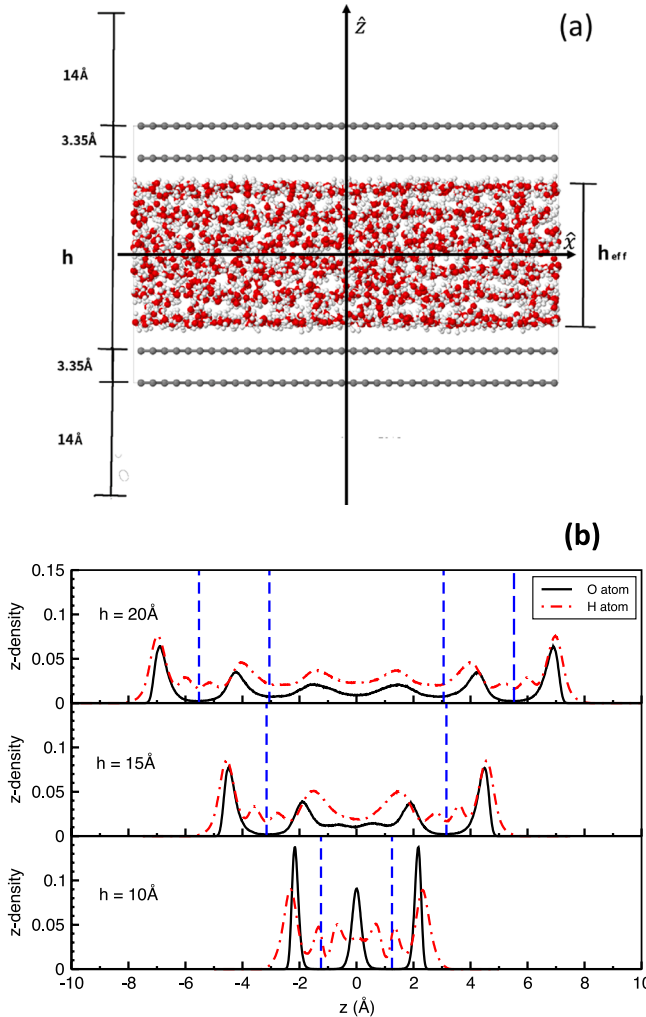


**Fig. 1.** (a) Simulation system for water confined within a graphite nanoslit. The slit width  $h$  is the distance between two inner C-atom plates and the effective slit width  $h_{\text{eff}}$  is the z-distance of space occupied by water molecules. The x- and y-axes are parallel to graphite plates and the z-axis is normal to the plate. (b) Z-density profile of water molecules confined within a graphite nanoslit. The black-solid and red-dash lines present the profiles of oxygen and hydrogen atoms, respectively. The vertical blue-dash lines indicate layer boundaries determined by the minima of O-atom profile, at  $|z| = 3.055$  and  $5.525 \text{ \AA}$  for  $h = 20 \text{ \AA}$ , at  $|z| = 3.155 \text{ \AA}$  for  $h = 15 \text{ \AA}$ , and at  $|z| = 1.245 \text{ \AA}$  for  $h = 10 \text{ \AA}$ . (For interpretation of the references to colour in this figure legend, the reader is referred to the web version of this article.)

varying the slit width from 20 to 10 Å with water density within the geometric space of a nanoslit close to that of liquid water at ambient conditions. The VDOS of nanoconfined water was dissected with the instantaneous-normal-mode (INM) analysis [27,28], which has been used extensively to study ultrafast dynamics and vibrational spectroscopy of bulk water at liquid and supercooled states [29–32]. The INM DOS of nanoconfined water can be formulated as contributions of water layers within a nanoslit. The paper is organized as follows: Sect. II describes simulations of confined system and layer structures of nanoconfined water obtained by our simulations. Sect. III portraits the INM analysis and VDOS of nanoconfined water. Sect. IV presents our results. Conclusions are given in Sect. V.

## 2. Simulation and layer structure

### 2.1. Molecular dynamics simulation

In our simulations, a graphite nanoslit was composed of four parallel C-atom plates with two layers (AA-stacking) separated at  $3.35 \text{ \AA}$  on each side of the slit as shown in Fig. 1(a), where C-atoms in a plate were frozen at hexagonal lattice sites of graphite and the slit width  $h$  was measured by the separation between two inner plates. The whole simulation system was inside a box subject to period boundary conditions, with box length  $L_x$  and  $L_y$  equal to  $44.27$  and  $46.86 \text{ \AA}$  of a graphite plate in the x- and y-direction, respectively. In the z-direction, the graphite plates within the simulation box were separated with an empty space of  $28 \text{ \AA}$  from their images, so that interactions between water molecules and their images in the z-direction were negligible.

By using the package LAMMPS [33], we performed MD simulations of water confined within a graphite nanoslit by two steps: First, we simulated bulk water of  $N$  molecules in a box with a size slightly smaller than the geometric space of a nanoslit described above, with the details given in [Supplemental Material](#). With molecules initially located at fcc lattice points, the bulk water was simulated in *NVT*-ensemble at  $300 \text{ K}$  with a time step of  $1 \text{ fs}$  for  $300 \text{ ps}$ . In the second step, the final state of bulk water was inputted into the graphite nanoslit as the initial configuration. Subject to repulsions from the graphite plates, confined water molecules were simulated in *NVT*-ensemble at  $300 \text{ K}$  with a time step of  $1 \text{ fs}$  for  $10 \text{ ns}$  for equilibrium. Then, the simulation was changed to *NVE*-ensemble with the same time step for  $1 \text{ ns}$  to collect data for analyses.

In our calculations, TIP4P/2005 rigid water model was adopted, where the model describes appropriately thermodynamic behaviors of bulk water [34]. The SHAKE algorithm was used to keep the rigidity of water molecule and the equations of motion were integrated with the Verlet algorithm. The hydrophobic interactions between water and graphite were described by the Lennard-Jones (LJ) potential of O-C atomic pairs, where the energy and length parameters  $\epsilon_{oc}$  and  $\sigma_{oc}$  follow the Lorentz-Berthelot mixing rules [35]:  $\epsilon_{oc} = \sqrt{\epsilon_{oo}\epsilon_{cc}}$  and  $\sigma_{oc} = (\sigma_{oo} + \sigma_{cc})/2$ , with values given in [Table S1 of Supplementary Material](#). The LJ potentials of O-O and O-C atomic pairs were truncated at  $12 \text{ \AA}$ , and the Coulombic interactions longer than this distance were calculated with the particle-particle and particle-mesh method in an accuracy of  $10^{-4}$  for bulk water and of  $10^{-5}$  for confined water [36]. All *NVT*-simulations were controlled by the Nose-Hoover thermostat with a time constant of  $0.1 \text{ ps}$  [37,38].

Our simulations were carried out for three nanoslits of width  $h = 20$ ,  $15$ , and  $10 \text{ \AA}$ , containing water molecules of number  $N = 1408$ ,  $1080$ , and  $720$ , respectively. Thus, the mass densities  $\rho_{\text{geo}}$  of the three confined waters within the nanoslit geometric space were  $1.015 \sim 1.038 \text{ g/cm}^3$ , which is close to that of liquid water at ambient conditions. The confinement effect can be obtained by comparing the properties of the three confined waters. Due to the hydrophobic interactions, water molecules within a nanoslit were generally restricted within an effective width  $h_{\text{eff}}$  estimated as [39]

$$h_{\text{eff}} = h - \frac{\sigma_{oc} + \sigma_{oo}}{2} \quad (1)$$

Within the restricted slit region, the effective mass density  $\rho_{\text{eff}}$  of confined water was nearly  $1.21$ ,  $1.32$ , and  $1.53 \text{ g/cm}^3$  for the nanoslit of  $h = 20$ ,  $15$ , and  $10 \text{ \AA}$ , respectively. Thus, the confined water in our simulations has a fixed number of molecules in an effective mass density higher than liquid water.

### 2.2. Layer structure

Obtained by our *NVE*-simulations, the z-density profiles of O- and H-atom are presented in Fig. 1(b), where the profiles are symmetric with

**Table 1**

Thickness  $d_l(\text{\AA})$ , average molecular number  $\bar{N}_l$ , mass density  $\rho_l(\text{g/cm}^3)$  of a water layer within a graphite nanoslit, and  $\chi_l$  in parentheses indicating the average molecular fraction of the layer.

| Slit width<br>$h$ | $d_l$ | Outer layer         |          | $d_l$ | Next layer          |          | Inner layer |                     |
|-------------------|-------|---------------------|----------|-------|---------------------|----------|-------------|---------------------|
|                   |       | $\bar{N}_l(\chi_l)$ | $\rho_l$ |       | $\bar{N}_l(\chi_l)$ | $\rho_l$ | $d_l$       | $\bar{N}_l(\chi_l)$ |
| 20 Å              | 2.860 | 235 (0.167)         | 1.181    | 2.470 | 218 (0.155)         | 1.273    | 6.110       | 502 (0.356)         |
| 15 Å              | 2.735 | 253 (0.234)         | 1.331    |       |                     |          | 6.310       | 574 (0.532)         |
| 10 Å              | 2.140 | 242 (0.336)         | 1.626    |       |                     |          | 2.490       | 236 (0.328)         |

**Table 2**

HB number  $n_{HB}$  of water molecule within a graphite nanoslit.  $n_{HB}$  was averaged over all molecules within a nanoslit or molecules of a single layer. The HBs of a layer were distinguished into intralayer and interlayer HBs. For the nanoslit of width 20 Å, the interlayer HBs of the next layer may connect to an outer layer (O) or the inner layer (I).

| Slit width | Conf. Mole. | Outer layer |       |       | Next layer |       |                     | Inner layer |       |       |
|------------|-------------|-------------|-------|-------|------------|-------|---------------------|-------------|-------|-------|
|            |             | All         | Intra | Inter | All        | Intra | Inter               | All         | Intra | Inter |
| 20 Å       | 3.628       | 3.476       | 2.612 | 0.864 | 3.703      | 1.823 | 0.926 (O) 0.955 (I) | 3.697       | 2.866 | 0.831 |
| 15 Å       | 3.612       | 3.470       | 2.609 | 0.860 |            |       |                     | 3.736       | 2.981 | 0.755 |
| 10 Å       | 3.361       | 3.325       | 2.244 | 1.077 |            |       |                     | 3.434       | 1.216 | 2.219 |

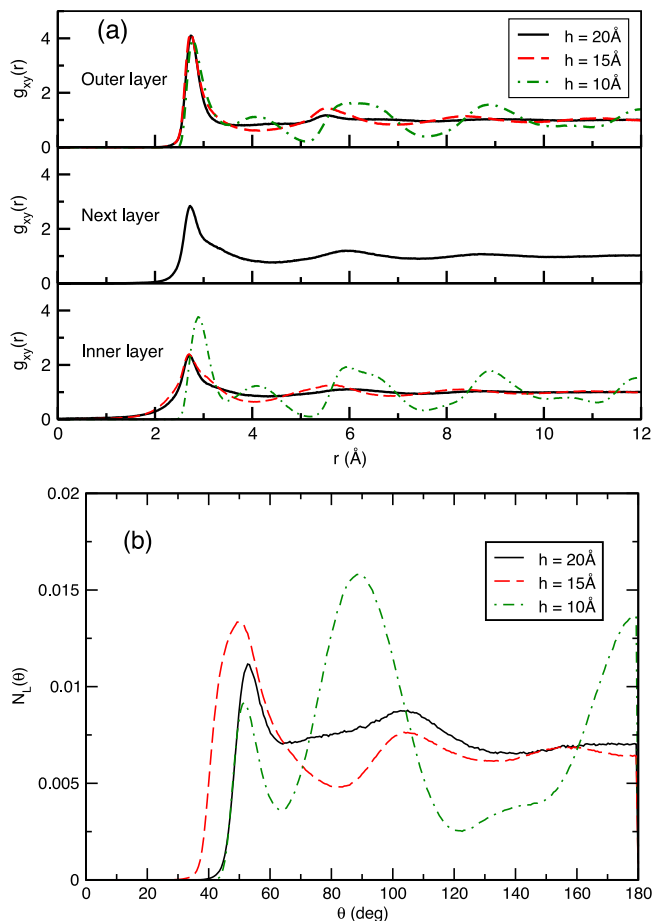


**Fig. 2.** In-plane structure of water layer within graphite nanoslits: (a) the lateral O-O RDF  $g_{xy}(r)$  of a layer and (b) the lateral O-O-O angle distribution  $N_L(\theta)$  of an outer layer. In (a), panels from top to bottom present the results of outer, next, and inner layers, and the black-solid, red-dash, and green-dot-dash lines are for nanoslits of width 20, 15, and 10 Å, respectively. In (b), the  $N_L(\theta)$  distribution was calculated with a neighborhood distance  $r_c$  at 3.485, 4.135, and 3.555 Å for the nanoslits of  $h = 20$ , 15, 10 Å, respectively, where  $r_c$  was set at the first minimum of  $g_{xy}(r)$  of the outer layer. (For interpretation of the references to colour in this figure legend, the reader is referred to the web version of this article.)

respect to the slit center at  $z = 0$ . The confined water formed layer structure parallel to graphite plates, with the layer boundaries determined at minima of the O-atom z-density profile. Within the nanoslit of  $h = 20\text{\AA}$ , confined water was distinguished into outer, next, and inner layers with increasing distance from a graphite wall. Within the other two nanoslits, confined water had only outer and inner layers, where the inner layer involves the central region of a nanoslit. In a remark, in the central region of the slit of width 15 Å, the O-atom z-density profile displayed small fluctuations but no corresponding fluctuation was found in the H-atom profile. The fluctuations in the O-atom profile were too small to be recognized as extra layers so that the confined water had four layers, in agreement with SPC/E water confined within the nanoslit of the same width [17].

The thicknesses of next and inner layers were estimated by the distance between two consecutive layer boundaries, whereas the outer-layer thickness was estimated by the distance from the first minimum of O-atom z-density profile to the limit set by the effective slit width, with the data of layer thickness  $d_l$  given in Table 1. Molecules within a nanoslit may cross back and forth the layer boundaries so that the O-atom number  $N_l$  of a water layer fluctuated in time and the time dependence of  $N_l$  is shown in Fig. S2 of Supplementary Material, where the molecular fluctuations were estimated about 1 ~ 2 percent for layers within nanoslits of  $h = 20$  and 15 Å and less than 1 percent for layers within the nanoslit of  $h = 10\text{\AA}$ . A time average of  $N_l$  over a simulation period of 60 ps gives the average number  $\bar{N}_l$  of O-atoms (or molecules) in a water layer. With  $\bar{N}_l$  and the layer thickness  $d_l$ , the mass density  $\rho_l$  of a layer was estimated and the data of the three nanoslits are given in Table 1. In general, the thickness of the outer layer decreases with the slit width, in consequence of a significant increase in its mass density. For the nanoslit of width 20 Å, the next layer, squeezed by the outer and inner layers, has a narrower width, making its mass density higher than its adjacent layers. For the nanoslit of width 10 Å, the outer layer has a density much higher than the inner layer.

Within a graphite nanoslit, H-atoms are closer to the confining wall than O-atoms. For an outer layer, the z-density profile of H-atom displays two peaks. For nanoslits of width 20 Å and 15 Å, the two H-atom peaks are quite asymmetric in shape, with the exterior H-atom profile mostly overlapping the O-atom one; the large overlap indicates that molecules in an outer layer have an OH-bond in preference to parallel the graphite plate. For the nanoslit of width 10 Å, the z-density profiles of an outer layer became sharper, with a reduce in the overlap between the H-atom and O-atom profiles, indicating that the strong squeezing from the graphite walls forces one OH-bond of an interfacial molecule to reorient toward the nearby graphite plate.

Due to the layer structure, the HB number  $n_{HB}$  of nanoconfined water depends on the slit width and the layer that the molecule is embedded in [13]. Tabulated in Table 2 are  $n_{HB}$  averaged over all confined molecules or molecules in a single layer. In general,  $n_{HB}$  of nanoconfined water is less than that of bulk water, where  $n_{HB}$  of TIP4P/2005 water is about 3.69 in terms of the geometric HB definition [40]. The  $n_{HB}$  of an outer layer is even lower; however, the next and inner layers within the nanoslits of width 20 and 15 Å have  $n_{HB}$  close to the bulk value, which is consistent with the results given in Ref. [23]. We distinguished the HBs of a single layer into intralayer and interlayer ones, which have the donor and acceptor molecules located in the same layer or belonging to two adjacent layers, respectively. The HB network of nanoconfined water can be characterized with the intralayer and interlayer HB numbers of its layers. For the nanoslit of width 10 Å, the intralayer HB number is reduced but the interlayer HB number increases, in comparison with the two nanosilts with a broader width.

### 2.3. In-plane structure of water layer

The in-plane structures of water layer within the three nanoslits are shown in Fig. 2(a) and 2(b), which present the lateral O-O radial distribution function (RDF)  $g_{xy}(r)$  and the lateral O-O-O angle distribution  $N_L(\theta)$  of an outer layer, respectively. For the three nanoslits,  $g_{xy}(r)$  of all layers exhibit a first peak near 2.72 Å. For  $h = 20$  Å,  $g_{xy}(r)$  of all layers have values around unity beyond the first peak. For  $h = 15$  Å,  $g_{xy}(r)$  of the outer and inner layers display shell structures and approach to unity at long distances, indicating a complete disorder in structure as projected onto the x-y plane. For the nanoslit of width 10 Å,  $g_{xy}(r)$  of outer and inner layers show strong oscillations, indicating a long-range order in the in-plane structure. Hence, the nanoconfined water was considered as in liquid-like states within the nanoslits of width 15 and 20 Å but in solid-like states within the nanoslit of 10 Å. The thermodynamic assignments for the three nanoconfined waters are consistent with their effective mass densities given in Table 1, according to the phase diagram of water confined within hydrophobic nanoslits [41].

For the slit width of 20 Å,  $N_L(\theta)$  displays a sharp peak near 53°, a wide one near 104°, and a weak maximum at 180° in relative to a broad background above 40°. The peak near 104° was attributed to the tetrahedral structure of molecular triplet, which has a central molecule connecting two neighbors via its donor HBs. The peak near 53° was resulted from the bisecting in the H-O-H bond angle of the central molecule of a molecular triplet by a fourth neighbor so that a rhombic structure is formed as shown in Fig. S3(a) of Supplementary Material. The maximum at 180° was caused by three collinear molecules with each one having one OH-bond in alignment. For the slit width of 15 Å,  $N_L(\theta)$  still broadly spreads with two peaks near 50° and 104°, and a maximum near 157°, whereas the peak near 50° increases in magnitude but the peak near 104° decreases, as compared with those peaks in  $N_L(\theta)$  of  $h = 20$  Å. The changes in the peak magnitudes in  $N_L(\theta)$  reveal that as reducing the slit width more rhombic structures in an outer layer were produced as shown in Fig. S3(b). The amount of rhombic structure was estimated about 3.1 and 5.7 percent for the slit width of 20 and 15 Å, respectively, with the estimations given in Supplementary Material. For the slit width of 10 Å, the distribution of  $N_L(\theta)$  changes dramatically, by displaying two main peaks near 90° and 180° and a smaller one near 50°, where the two main peaks were resulted from the majority in square structure and the small peak arises from the minority in rhombic structure, which had an amount about 2 percent as in Fig. S3(c). Thus, as reducing the slit width from 20 to 10 Å, the in-plane structure of an outer layer exhibits a transition from liquid-like to solid-like state, which is consistent with the thermodynamic assignments for the three nanoconfined waters described above.

## 3. Intermolecular vibration of nanoconfined water

### 3.1. Instantaneous normal mode formalism

The total potential energy of water confined within a graphite nanoslit involves the potential energy  $V^{(W)}$  of water molecules and the hydrophobic interaction  $V_{Hydro}$  between water and graphite. In comparison to the Hessian  $H^{(W)}$  of bulk water, the Hessian  $H^{(CW)}$  of confined water has an extra term due to the hydrophobic interaction, with the elements of  $H^{(CW)}$  expressed as

$$H_{k\mu,l\nu}^{(CW)} = H_{k\mu,l\nu}^{(W)} + \frac{\partial^2 V_{Hydro}}{\partial z_{k\mu} \partial z_{l\nu}}, \text{ with } k, l = 1, \dots, N, \text{ and } \mu, \nu = 1, \dots, 6 \quad (2)$$

where  $z_{k\mu}$  is the mass-weighted coordinates, with  $\mu = 1, 2, 3$ , describing the center-of-mass (CM) position of molecule  $k$  in the Lab. frame and, with  $\mu = 4, 5, 6$ , depicting the short-time rotation of the molecule in its instantaneous molecular frame.

The diagonalization of  $H^{(CW)}$  at confined water configuration  $\mathbf{R}_0$  gives  $6N$  eigenvalues  $\lambda_\alpha$ , with  $\alpha = 1, 2, \dots, 6N$ , where the square root of  $\lambda_\alpha$  gives the INM frequency  $\omega_\alpha(\mathbf{R}_0)$ . The normalized eigenvector of INM  $\alpha$  has  $6N$ -components  $U_{\alpha,k\mu}(\mathbf{R}_0)$  associated with each  $z_{k\mu}$ . In terms of the degree-of-freedom projector defined as [29]

$$P_{a\mu} = \sum_{k=1}^N (U_{\alpha,k\mu}(\mathbf{R}_0))^2, \quad (3)$$

The INM density of states (DOS) for each molecular degree of freedom is given as

$$D_\mu^{INM}(\omega) = \left\langle \frac{1}{6N} \sum_{\alpha=1}^{6N} P_{a\mu} \delta(\omega - \omega_\alpha(\mathbf{R}_0)) \right\rangle, \quad (4)$$

where the angular brackets stand for an ensemble average. The total INM DOS  $D_{tot}^{INM}(\omega)$  is a sum of translational and rotational INM DOS: The translational INM DOS  $D_{cm}^{INM}(\omega)$ , contributed from molecular CM motions, is a sum of  $D_\mu^{INM}(\omega)$  with  $\mu = 1$  to 3, and the rotational INM DOS  $D_{rot}^{INM}(\omega)$  is a sum of  $D_\mu^{INM}(\omega)$  associated with each molecular axis. Here,  $D_{tot}^{INM}(\omega)$  is normalized to one and  $D_\mu^{INM}(\omega)$  of each degree of freedom is normalized to 1/6. The component  $D_{cm,\parallel}^{INM}(\omega)$  and  $D_{cm,\perp}^{INM}(\omega)$  of  $D_{cm}^{INM}(\omega)$  are related to molecular CM motions parallel and perpendicular to the confining wall, respectively, where  $D_{cm,\parallel}^{INM}(\omega)$  is an average of  $D_1^{INM}(\omega)$  and  $D_2^{INM}(\omega)$  and  $D_{cm,\perp}^{INM}(\omega) = D_3^{INM}(\omega)$ .

As described in the previous section, water confined within a graphite nanoslit forms layer structure so that molecules can be categorized into different layers, specified with  $l = Outer, Next, Inner, \dots$ . The INM projector associated with molecules of a layer is defined as [31]

$$P_{a\mu}^{(l)} = \sum_{k=1}^N (U_{\alpha,k\mu}(\mathbf{R}_0))^2 \Theta_k(l), \quad (5)$$

where the molecular selector  $\Theta_k(l)$  of  $l$ -layer is given as

$$\Theta_k(l) = \begin{cases} 1, & \text{if molecule } k \text{ is in layer } l, \\ 0, & \text{otherwise} \end{cases} \quad (6)$$

In terms of  $P_{a\mu}^{(l)}$ , the INM DOS contributed from molecules of  $l$ -layer is given as

$$D_\mu^{INM,l}(\omega) = \frac{1}{N_l} \sum_{\alpha=1}^{6N} P_{a\mu}^{(l)} \delta(\omega - \omega_\alpha(\mathbf{R}_0)), \quad (7)$$

where  $N_l$  is the molecular number of  $l$ -layer and  $D_\mu^{INM,l}(\omega)$  is normalized to unity. One sum rule of  $P_{a\mu}^{(l)}$  gives the relation [31]

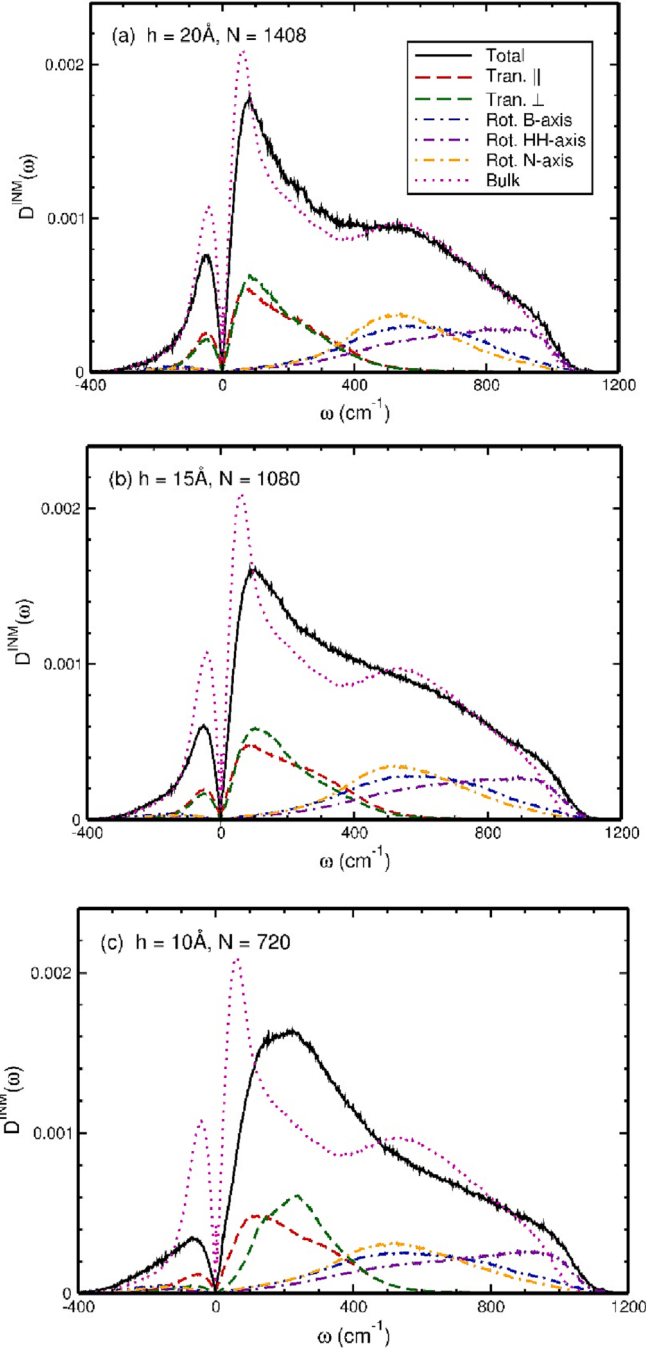


**Fig. 3.** INM DOS of water confined within a graphite nanoslit at a width: (a) 20 Å, (b) 15 Å, and (c) 10 Å. The black solid lines are the total DOS  $D_{\text{tot}}^{\text{INM}}(\omega)$ . The red and green dash lines are  $D_{\text{cm},||}^{\text{INM}}(\omega)$  and  $D_{\text{cm},\perp}^{\text{INM}}(\omega)$ , the parallel and perpendicular components of translational INM DOS, respectively. The blue, violet, and orange dot-dash lines are the rotational INM DOS associated with the molecular dipole axis, the axis connecting H-atoms, and the axis normal to molecular plane, respectively. The magenta dot lines are the total INM DOS of TIP4P/2005 liquid water at 1 atm and 300 K. (For interpretation of the references to colour in this figure legend, the reader is referred to the web version of this article.)

$$D_{\mu}^{\text{INM}}(\omega) = \frac{1}{6} \sum_{l=\text{layer}} \chi_l D_{\mu}^{\text{INM},l}(\omega), \quad (8)$$

where  $\chi_l = \bar{N}_l/N$  is the average molecular fraction of  $l$ -layer within a graphite nanoslit.

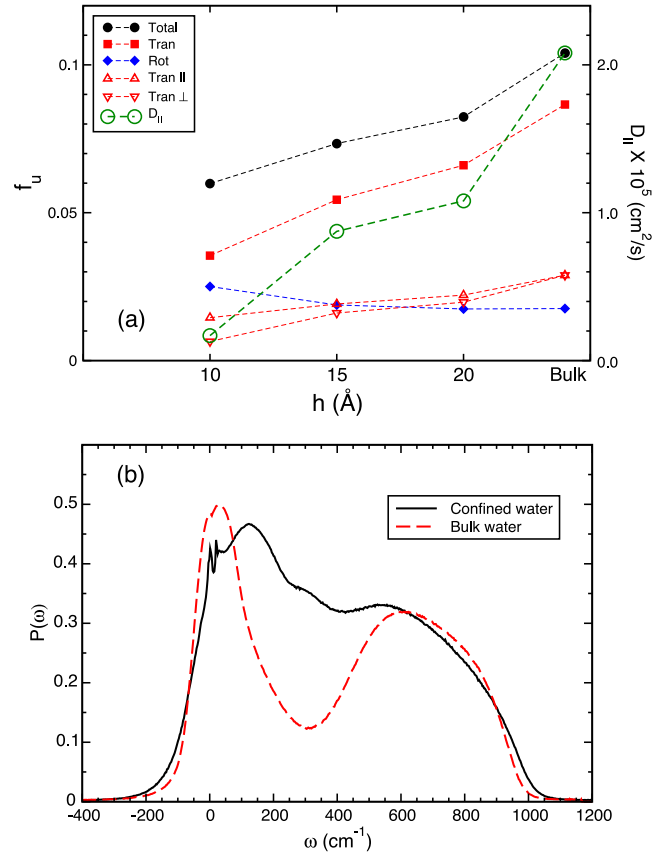


**Fig. 4.** (a) Im-INM fraction of nanoconfined water in variation with the width  $h$  of a graphite nanoslit. The black circles, red squares, and blue diamonds indicate the fractions of total, translational, and rotational Im-INMs, respectively. The upper and down triangles are, respectively, the fractions of parallel and perpendicular translational components. The green open circles indicate the lateral self-diffusion coefficient  $D_{\parallel}$  of nanoconfined water, with a scale referred to the right axis. The dash lines guide the eye for the data set, with the data at the right-hand side for TIP4P/2005 liquid water at ambient conditions. (b) INM participation ratio as a function of frequency for water confined within a graphite nanoslit of width 10 Å (black solid line) and for liquid water (red dash line). (For interpretation of the references to colour in this figure legend, the reader is referred to the web version of this article.)

### 3.2. Vibrational density of states

For molecular liquids, VDOS  $D_{\text{cm}}(\omega)$  is the Fourier-cosine transform of the normalized velocity autocorrelation function (VACF)  $C_{\text{cm}}(t)$ ,

$$D_{\text{cm}}(\omega) = \frac{2}{\pi} \int_0^\infty C_{\text{cm}}(t) \cos(\omega t) dt, \quad (9)$$

where  $C_{\text{cm}}(t)$  is related to molecular CM velocity in the Lab. frame and can be obtained via MD simulations. Due to the nanoslit geometry,  $C_{\text{cm}}(t)$  can be separated into  $C_{\text{cm},||}(t)$  and  $C_{\text{cm},\perp}(t)$  associated with CM-velocity components parallel and perpendicular to the confining wall, respectively, and  $D_{\text{cm},||}(\omega)$  and  $D_{\text{cm},\perp}(\omega)$  are the corresponding transformation of  $C_{\text{cm},||}(t)$  and  $C_{\text{cm},\perp}(t)$ . Supposed that the parallel and perpendicular components of molecular CM velocity are independent,  $D_{\text{cm}}(\omega) = (2D_{\text{cm},||}(\omega) + D_{\text{cm},\perp}(\omega))/3$ , where all VDOSs are normalized to unity.

The layer VACF was calculated for molecules initially in a layer, though molecules may cross over layer boundaries and diffuse to other layers some time later. As shown in Fig. S5, the decay times for the VACFs of nanoconfined water are roughly 0.5 ps. As aforementioned, the

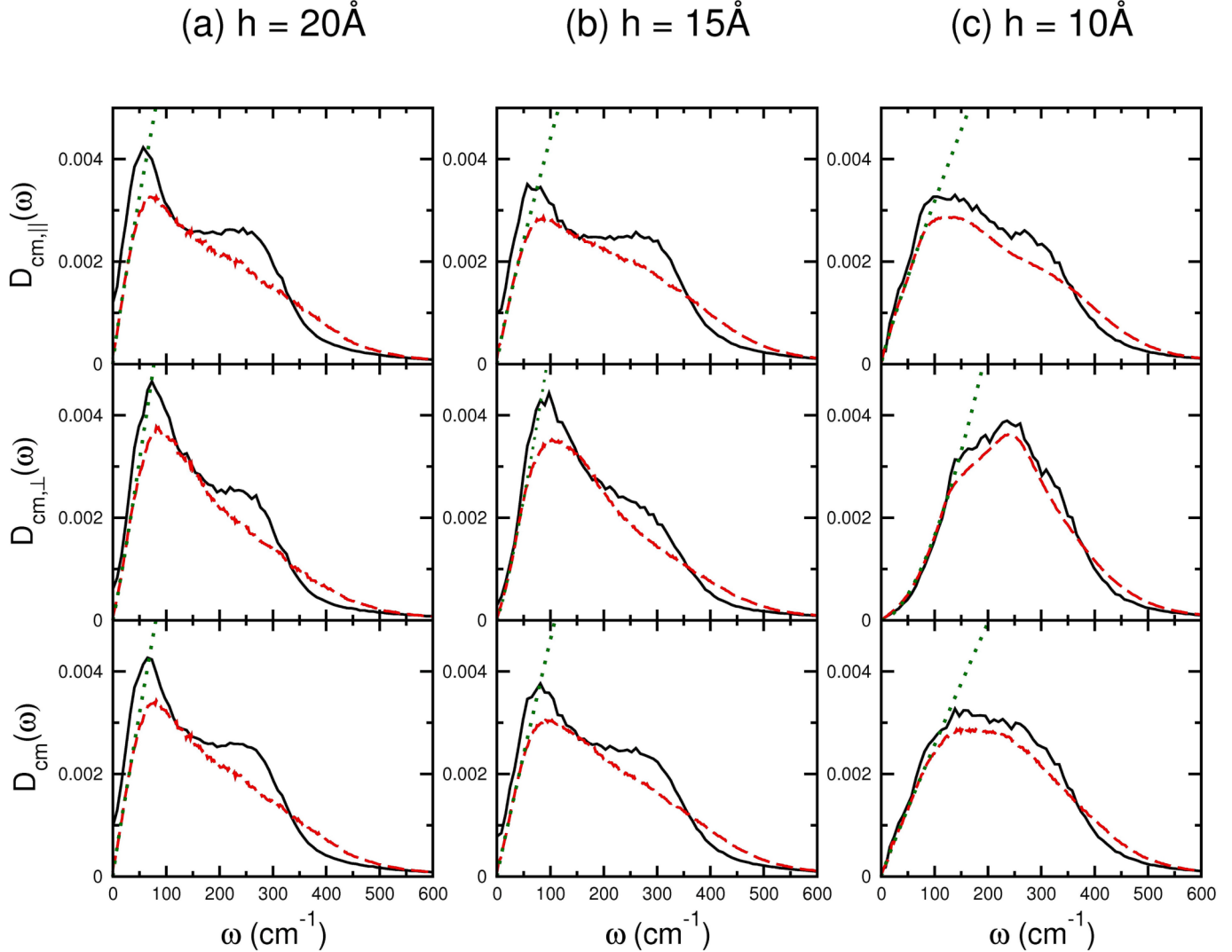


**Fig. 5.** Comparison between VDOS (black-solid lines) and translational INM DOS in the real lobe (red-dash lines) of water confined within graphite nanoslits. The real-lobe INM DOS was normalized to unity. The columns from left to right are for nanoslits of width 20, 15, 10 Å, respectively. The panels from top to bottom show comparisons of parallel component  $D_{cm,||}(\omega)$ , perpendicular component  $D_{cm,\perp}(\omega)$ , and full VDOS  $D_{cm}(\omega)$  with the corresponding INM DOS. The green-dot lines indicate the fitting results for the low-frequency INM DOS by using a power-law function  $A\omega^n$ . (For interpretation of the references to colour in this figure legend, the reader is referred to the web version of this article.)

fluctuation of molecular number in a layer is extremely small and, thus, yields negligible influence on the VACF of the layer.

Via the Green-Kubo formula [35], the value of  $D_{cm,||}(\omega)$  at  $\omega = 0$  gives the lateral self-diffusion coefficient  $D_{||}$  of molecular transport parallel to the slit wall, manifesting the parallel mobility of confined molecules. The magnitude of  $D_{||}$  serves an indicator for solid-like or liquid-like state of nanoconfined water, with the self-diffusion coefficient of bulk water as a reference. In the INM theory of liquid, the translational INM DOS  $D_{cm}^{INM}(\omega)$  is approximated to VDOS  $D_{cm}(\omega)$  but has a broader spectrum for no motional narrowing effect [42]. However, as lowering the temperature of a substance to its solid state,  $D_{cm}(\omega)$  and  $D_{cm}^{INM}(\omega)$  are expected to agree more and more with each other.

#### 4. Results and discussion

The VACF  $C_{cm}(t)$ ,  $C_{cm,||}(t)$ , and  $C_{cm,\perp}(t)$  of water confined within each of the three graphite nanoslits are shown in Fig. S5 of Supplementary Material. Our results are consistent with previous simulations [17]. Specially, for  $h = 10 \text{ \AA}$ ,  $C_{cm,\perp}(t)$  almost decays out after a strong oscillation within the first 0.1 ps. The VDOS  $D_{cm}(\omega)$ ,  $D_{cm,||}(\omega)$ , and  $D_{cm,\perp}(\omega)$

are shown in the insets of Fig. S5, with the result of liquid water as a reference. The VDOS of bulk water shows a peak near  $60 \text{ cm}^{-1}$  and a maximum around  $225 \text{ cm}^{-1}$ , which are assigned to the O-O-O bending motion and O-O stretching vibration, respectively [43]. In reference to bulk water,  $D_{cm}(\omega)$  of nanoconfined water has a blue shift increasing with the confinement. At  $h = 20 \text{ \AA}$  and  $15 \text{ \AA}$ , all VDOSS of nanoconfined water display a low-frequency peak, having a blue shift and reduced magnitude as decreasing the slit width, whereas around  $225 \text{ cm}^{-1}$   $D_{cm,||}(\omega)$  displays a weak maximum and  $D_{cm,\perp}(\omega)$  changes to a shoulder. At  $h = 10 \text{ \AA}$ ,  $D_{cm}(\omega)$  exhibits a broad plateau and  $D_{cm,||}(\omega)$  shows a wide spectrum with a maximum and a shoulder near  $100$  and  $300 \text{ cm}^{-1}$ , respectively, but the behavior of  $D_{cm,\perp}(\omega)$  changes to a mixture of solid-like phonon spectrum at low and intermediate frequencies and a long tail at high frequencies, where the solid-like spectrum presents a power-law dependence followed with a cusp, which will be discussed later.

Estimated by  $D_{cm,||}(\omega)$  at  $\omega = 0$ , the lateral self-diffusion coefficients  $D_{||}$  of nanoconfined water are roughly  $1.08$ ,  $0.87$ , and  $0.17 \times 10^{-5} \text{ cm}^2/\text{s}$  for the slit width of  $20$ ,  $15$ , and  $10 \text{ \AA}$ , respectively. By referring to the self-diffusion coefficient of TIP4P/2005 water, which is near  $2.06 \times$

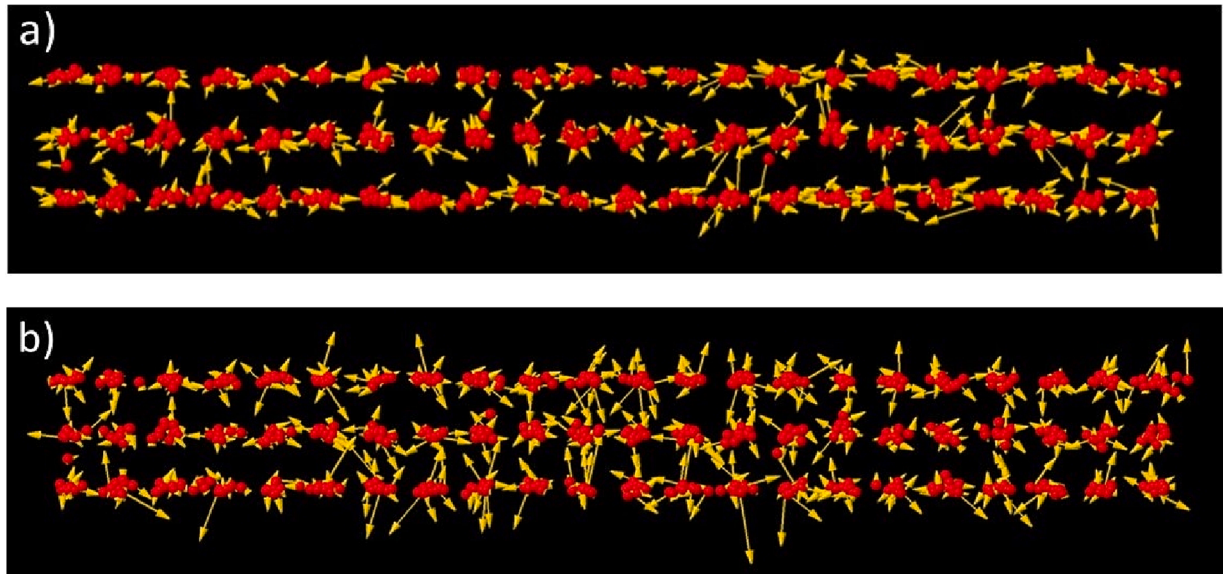


**Fig. 6.** Side view of INM-eigenvector for water molecules confined within graphite nanoslit of width 10 Å: (a)  $\omega \approx 60 \text{ cm}^{-1}$  and (b)  $\omega \approx 225 \text{ cm}^{-1}$ . The nanoconfined water consists of triplet molecular layers within a width  $h_{\text{eff}} \approx 6.78 \text{ \AA}$ . The red spheres indicate O-atoms, but H-atoms were removed out for clarity. The arrows specify the relative magnitudes of eigenvector component associated with each molecule. (For interpretation of the references to colour in this figure legend, the reader is referred to the web version of this article.)

$10^{-5} \text{ cm}^2/\text{s}$  at ambient conditions [34], the nanoconfined water was considered as in liquid-like states within the nanoslits of width 20 and 15 Å but in solid-like states for the slit width of 10 Å. The assignments are consistent with their layer structures and also with the liquid-to-solid transition of bilayer water, where  $D_{||}$  decreases in one order of magnitude during the transition as calculated with the same water model [44].

Fig. 3 presents the INM DOS of nanoconfined water. In comparison to bulk water, the INM DOS  $D_{\text{tot}}^{\text{INM}}(\omega)$  of nanoconfined water generally has a reduction in the imaginary lobe and a blue shift in the real lobe, where the peak, originally near  $60 \text{ cm}^{-1}$  for bulk water, shifts to  $80 \text{ cm}^{-1}$  for the nanoslit of width 20 Å. One cause for the change in  $D_{\text{tot}}^{\text{INM}}(\omega)$  is the increment in effective water density due to the confinement. For the nanoslit of  $h = 20 \text{ \AA}$ , the rotational INM DOS  $D_{\text{rot}}^{\text{INM}}(\omega)$ , mainly above  $400 \text{ cm}^{-1}$  in the real lobe, is similar in frequency range as that of bulk water, but the translational INM DOS  $D_{\text{cm}}^{\text{INM}}(\omega)$ , mostly below  $400 \text{ cm}^{-1}$ , has a blue shift. At  $h = 15 \text{ \AA}$ ,  $D_{\text{rot}}^{\text{INM}}(\omega)$  extends somewhat over the high-frequency limit of bulk water, and the translational component  $D_{\text{cm},||}^{\text{INM}}(\omega)$  and  $D_{\text{cm},\perp}^{\text{INM}}(\omega)$  have a triangular shape as that of a LJ atomic fluid [27,28,45], with  $D_{\text{cm},\perp}^{\text{INM}}(\omega)$  having an enhancement from 80 to  $200 \text{ cm}^{-1}$ . As reducing the slit width to 10 Å,  $D_{\text{rot}}^{\text{INM}}(\omega)$  still has a triangular shape but the behavior of  $D_{\text{cm},\perp}^{\text{INM}}(\omega)$  changes dramatically and is similar to VDOS  $D_{\text{cm},\perp}(\omega)$ .

The imaginary INMs (Im-INMs) of a liquid are unstable modes resulted from the negative curvatures of shoulder or double-well potential energy profile, where the ones associated with the double-well potential may cause the liquid to diffuse by crossing over barriers between adjacent basins in potential energy landscape [46]. For nanoconfined water, the variation of Im-INM fraction  $f_u$  with the width of a graphite nanoslit is presented in Fig. 4(a). As decreasing the slit width, the fraction of translational Im-INMs decreases but that of rotational Im-INMs increases, whereas the total Im-INM fraction still decreases with the slit width. In liquid states of nanoconfined water within the nanoslits of width 15 and 20 Å, the fraction of translational Im-INM is almost proportional to  $D_{||}$ , and this is consistent with the INM theory of 3D liquid. The proportionality can be realized as that  $D_{||}$  is caused by molecular random motions within a graphite nanoslit and, microscopically, the random motions are related to perpendicular molecular translations.

The INM participation ratio  $P(\omega)$  indicates the ratio of molecules participating in an INM [29,47] and can be obtained by averaging the participation ratio  $R_\alpha$  of INMs within a frequency window centered at  $\omega$ , where

$$R_\alpha = \left( N \sum_{k=1}^N \left( \sum_{\mu=1}^6 (U_{\alpha,k\mu}(\mathbf{R}_0))^2 \right)^2 \right)^{-1}. \quad (10)$$

The INMs can be characterized as localized or extended modes, where  $P(\omega)$  scales inversely with  $N$  for the former and is of order of unity for the latter. The  $P(\omega)$  of bulk water and nanoconfined water are presented in Fig. 4(b). For both cases,  $P(\omega)$  decays monotonously with increasing imaginary frequency, indicating that Im-INMs change from extension in space to localization with increasing frequency. For bulk water,  $P(\omega)$  in the real lobe shows a deep near  $300 \text{ cm}^{-1}$  with a value about 0.12, where the translational and rotational INM DOS are dominated below and above this frequency, respectively [32]. However, for water confined within the nanoslit of width 10 Å, there is no deep appearing in  $P(\omega)$ , as a result of the blue shift of translational INM DOS. Thus, except for those with extremely high frequencies, the real-frequency INMs of nanoconfined water are extended over all molecules within the nanoslit and the most extended INMs occur near  $125 \text{ cm}^{-1}$ , rather than near zero frequency as for bulk water. Hence, the translational INMs of water confined within a nanoslit of width 10 Å are collective in nature, possibly, due to its solid-like structure.

Comparisons between VDOS and translational INM DOS in the real lobe of nanoconfined water are shown in Fig. 5, where all VDOS and INM DOS are individually normalized to unity. For nanoslits of width 15 and 20 Å, a substantial deviation between INM DOS and VDOS is mainly resulted from the absence of motional narrowing effect in INM DOS, where the derivation is more prominent to the parallel component. But, for the nanoslit at  $h = 10 \text{ \AA}$ , the behaviors of VDOS and INM DOS become consistent with each other. We fit the low- $\omega$  translational INM DOS by using a power-law function  $A\omega^\eta$ . Our results indicate that the exponent  $\eta$  characterizing  $D_{\text{cm}}^{\text{INM}}(\omega)$  at low frequencies is near 0.95 for the three nanoconfined waters, where the linear low-frequency behavior of INM DOS has been evidenced as the universal law for 3D liquids [48,49]. Here, we extend numerically the universal law to nanoconfined water.

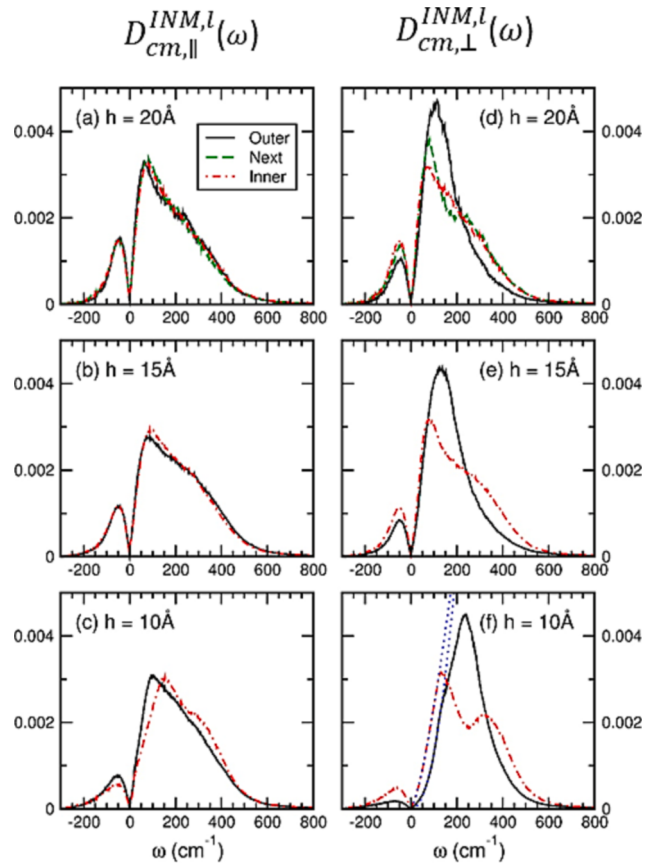


**Fig. 7.** Parallel (left column) and perpendicular (right column) components of translational INM DOS calculated for water layers within a graphite nanoslit. The panels from top to bottom are shown for the nanoslits of width 20, 15, 10 Å, respectively. The black-solid, green-dash, and red-dot-dash lines are for the outer, next, and inner layers within a nanoslit, respectively. All DOSs are normalized to unity. In (f), the blue-dot lines are the power-law fitting for low-frequency INM DOS in the real lobe. (For interpretation of the references to colour in this figure legend, the reader is referred to the web version of this article.)

However, the  $\eta$ -value of the parallel component  $D_{cm,||}^{INM}(\omega)$  was found to be smaller than one, roughly  $0.87 \sim 0.9$ , for nanoconfined waters studied, whereas the  $\eta$ -value of the perpendicular component  $D_{cm,\perp}^{INM}(\omega)$  depends on the slit width and is near 1.1, 1.2, and 1.7 for  $h = 20, 15$ , and 10 Å, respectively. Particularly,  $D_{cm,\perp}^{INM}(\omega)$  at  $h = 10\text{ \AA}$  shows a power-law behavior up to a cusp near  $135\text{ cm}^{-1}$  and, then, ascends linearly to a summit around  $250\text{ cm}^{-1}$ , beyond which the DOS decays exponentially. To understand this naive behavior of DOS, the INM-eigenvector profile is helpful. The side views of INM eigenvector with  $\omega \approx 60$  and  $225\text{ cm}^{-1}$  are presented in Fig. 6 and their projections on an interfacial layer are shown in Fig. S6 of Supplementary Material. Indicated by these figures, the INM-eigenvector of  $\omega \approx 60\text{ cm}^{-1}$  has relatively large in-layer but small out-of-layer components, whereas the eigenvector of  $\omega \approx 225\text{ cm}^{-1}$  has large out-of-layer components. Inspired with these inputs, we give an explanation for the behavior of  $D_{cm,\perp}^{INM}(\omega)$ : By considering the nanoconfined water as a quasi-2D slab of a width  $h_{eff} \approx 6.78\text{ \AA}$ , the power-law behavior at low frequencies arises from small-amplitude out-of-layer molecular vibrations, similar as transverse acoustic waves propagating in parallel to the slab, and the summit around  $250\text{ cm}^{-1}$  is resulted from stretching vibrations between O-atoms in adjacent layers, akin to longitudinal optical phonons in solids but limited to propagate by the confinement.

The parallel and perpendicular components of layer translational

INM DOS  $D_{cm}^{INM}(\omega)$  are shown in Fig. 7 for the three nanoconfined waters. According to Eq. (8), the contributions of outer, next, and inner layers to  $D_{cm}^{INM}(\omega)$  are weighted by their molecular fractions  $\chi_i$  with data given in Table 1, where the numbers of outer and next layers should be double due to the symmetry of confined water with respect to the line at  $z = 0$ . Within a nanoslit, the parallel component of layer INM DOS is almost the same for all layers, indicating that the influence of graphite walls on in-layer molecular vibrations is similar for all layers. Specially, the INM DOS of the inner layer exhibits a weak hump near  $250 \sim 300\text{ cm}^{-1}$  in the real lobe, where the INM DOS of bulk water is enhanced with the number of HBs connecting to a molecule [50], and the hump grows to a shoulder as reducing the slit width to 10 Å, where the inner molecules have more HBs than the interfacial ones as given in Table 2.

The perpendicular component of layer INM DOS,  $D_{cm,\perp}^{INM,l}(\omega)$ , behaves differently for the outer, next, and inner layers. For nanoslits of  $h = 20$  and 15 Å,  $D_{cm,\perp}^{INM,l}(\omega)$  of the outer layer has a higher peak near  $100\text{ cm}^{-1}$  but that of the inner layer is enhanced above  $250\text{ cm}^{-1}$  such that  $D_{cm,\perp}^{INM,l}(\omega)$  of the next layer within the nanoslit of width 20 Å displays a shoulder near  $230\text{ cm}^{-1}$ , where the next-layer molecules have slightly more HBs. For the slit width of 10 Å,  $D_{cm,\perp}^{INM,l}(\omega)$  of the outer layer has a single peak shifting to  $230\text{ cm}^{-1}$ , but  $D_{cm,\perp}^{INM,l}(\omega)$  of the inner layer shows two maxima near  $135$  and  $330\text{ cm}^{-1}$ , where molecules have more interlayer HBs than intralayer ones. In the real lobe,  $D_{cm,\perp}^{INM,l}(\omega)$  of the outer and inner layers have different low-frequency behaviors, characterized with the  $\eta$ -exponent near 2.13 and 1.36, respectively. This indicates that at low-frequency intermolecular vibrations the outer-layer molecules have smaller perpendicular amplitudes than the inner-layer molecules. As summing the layer contributions together to give  $D_{cm,\perp}^{INM}(\omega)$ , the different behaviors in  $D_{cm,\perp}^{INM,l}(\omega)$  between the outer and inner layers give rise to the cusp near  $135\text{ cm}^{-1}$  in  $D_{cm,\perp}^{INM}(\omega)$  at  $h = 10\text{ \AA}$  shown in Fig. 5.

## 5. Conclusions

In this paper, we used MD simulations to study layer structure and intermolecular vibrations of water confined within graphite nanoslits. The confinement effect was investigated by varying the slit width from 20 to 10 Å, with water density in the geometric slit space close to that of liquid water at ambient conditions. In our simulations, nanoconfined water is a close system with a fixed molecular number and, therefore, has a high effective density caused by the hydrophobic interactions from the graphite walls. Generally, water confined within a graphite nanoslit formed layer structure, where nanoconfined water was found in liquid-like states as the slit width was 20 and 15 Å but had a structural transition to solid-like states as the slit width was reduced to 10 Å. Due to the layer structure, the HB network of nanoconfined water is characterized with intralayer (in-layer) and interlayer (out-of-layer) HB numbers, which vary with the slit width and depend on the layer distance from a nearby graphite wall. As reducing the slit width, water layers within a graphite nanoslit tend to have more interlayer but less intralayer HBs.

In comparison to bulk water, the VDOS of nanoconfined water has a blue shift in frequency with decreasing the slit width. The confinement makes the INM DOS of nanoconfined water a reduction in the imaginary lobe and a blue shift in the real lobe. The translational INMs of nanoconfined water are generally collective in nature and the INM DOS in the real lobe shows a linear behavior at low frequencies, in agreement with the INM theory for 3D liquids. But, the components of translational INM DOS parallel and perpendicular to the confining wall display different low-frequency behaviors, characterized with a power-law exponent less and larger than one, respectively. The different behaviors are resulted from the slit confinement, which causes low-frequency intermolecular vibrations within a nanoslit to have anisotropic amplitude distributions, with large in-layer but small out-of-layer components. This confinement

effect becomes more prominent as reducing the slit width to nanoscales and is more significant for molecules interfacial to a graphite wall than those in the inner of a nanoslit.

## CRediT authorship contribution statement

**Yu-Wei Kuo:** Software, Validation, Data curation. **Chi-Wei Wang:** Software, Formal analysis, Data curation. **Ping-Han Tang:** Conceptualization, Methodology, Software. **Ten-Ming Wu:** Conceptualization, Methodology, Resources, Writing – original draft, Writing – review & editing.

## Declaration of Competing Interest

The authors declare that they have no known competing financial interests or personal relationships that could have appeared to influence the work reported in this paper.

## Data availability

Data will be made available on request.

## Acknowledgements

TM Wu acknowledges supports from Ministry of Science and Technology, Taiwan under Grant No. MOST 110-2112-M-A49-021 and MOST 111-2112-M-A49-022.

## Appendix A. Supplementary data

Supplementary data to this article can be found online at <https://doi.org/10.1016/j.cplett.2023.140612>.

## References

- [1] N.E. Levinger, Water in confinement, *Science* 298 (5599) (2002) 1722–1723.
- [2] C.I. Lynch, S. Rao, M.S.P. Sansom, Water in nanopores and biological channels: a molecular simulation perspective, *Chem. Rev.* 120 (2020) 10298.
- [3] D. Muñoz-Santiburcio, D. Marx, Confinement-controlled aqueous chemistry within nanometric slit pores, *Chem. Rev.* 121 (2021) 6293.
- [4] B. Radha, A. Esfandiari, F.C. Wang, A.P. Rooney, K. Gopinadhan, A. Keerthi, A. Mishchenko, A. Janardanan, P. Blake, L. Fumagalli, M. Lozada-Hidalgo, S. Garaj, S.J. Haigh, I.V. Grigorieva, H.A. Wu, A.K. Geim, Molecular transport through capillaries made with atomic-scale precision, *Nature* 538 (2016) 222.
- [5] L. Fumagalli, A. Esfandiari, R. Fabregas, S. Hu, P. Ares, A. Janardanan, Q. Yang, B. Radha, T. Taniguchi, K. Watanabe, G. Gomila, K.S. Novoselov, A.K. Geim, Anomalously low dielectric constant of confined water, *Science* 360 (2018) 1339.
- [6] Y. Liu, Y. Zhao, X. Zhang, X. Huang, W. Liao, Y. Zhao, MoS<sub>2</sub>-based membranes in water treatment and purification, *Chem. Eng. J.* 422 (2021), 130082.
- [7] J.K. Holt, H.G. Park, Y. Wang, M. Stadermann, A.B. Artyukhin, C.P. Grigoropoulos, A. Noy, O. Bakajin, Fast mass transport through sub-2-nanometer carbon nanotubes, *Science* 312 (2006) 1034.
- [8] R.R. Nair, H.A. Wu, P.N. Jayaram, I.V. Grigorieva, A.K. Geim, Unimpeded permeation of water through helium-leak-tight graphene-based membranes, *Science* 335 (2012) 442.
- [9] N. Giovambattista, P.J. Rossky, P.G. Debenedetti, Phase transitions induced by nanoconfinement in liquid water, *Phys. Rev. Lett.* 102 (2009), 050603.
- [10] K. Koga, H. Tanaka, X.C. Zeng, First-order transition in confined water between high-density liquid and low-density amorphous phases, *Nature* 408 (2000) 564.
- [11] C.Y. Lee, J.A. McCammon, P.J. Rossky, The structure of liquid water at an extended hydrophobic surface, *J. Chem. Phys.* 80 (1984) 4448.
- [12] P. Hirunsit, P.B. Balbuena, Effects of confinement on water structure and dynamics: a molecular simulation study, *J. Phys. Chem. C* 111 (2007) 1709.
- [13] S. Ruiz-Barragan, D. Muñoz-Santiburcio, D. Marx, Nanoconfined water within graphene slit pores adopts distinct confinement-dependent regimes, *J. Phys. Chem. Lett.* 10 (2019) 329.
- [14] G. Algara-Siller, O. Lehtinen, F.C. Wang, R.R. Nair, U. Kaiser, H.A. Wu, A.K. Geim, I.V. Grigorieva, Square ice in graphene nanocapillaries, *Nature* 519 (7544) (2015) 443–445.
- [15] S. Singla, E. Anim-Danso, A.E. Islam, Y. Ngo, S.S. Kim, R.R. Naik, A. Dhinojwala, Insight on structure of water and ice next to graphene using surface-sensitive spectroscopy, *ACS Nano* 11 (5) (2017) 4899–4906.
- [16] J. Bai, X.C. Zeng, Polymorphism and polyamorphism in bilayer water confined to slit nanopore under high pressure, *Proc. Natl. Acad. Sci. U.S.A.* 109 (2012) 21240.
- [17] H. Mosaddeghi, S. Alavi, M.H. Kowsari, B. Najafi, Simulations of structural and dynamic anisotropy in nano-confined water between parallel graphite plates, *J. Chem. Phys.* 137 (2012), 184703.
- [18] J. Jiang, Y. Gao, W. Zhu, Y. Liu, C. Zhu, J.S. Francisco, X.C. Zeng, First-principles molecular dynamics simulations of the spontaneous freezing transition of 2D water in a nanoslit, *J. Am. Chem. Soc.* 143 (2021) 8177.
- [19] M. Abbaspour, H. Akbarzadeh, S. Salemi, E. Jalalitalab, Density-dependent phase transition in nano-confinement water using molecular dynamics simulation, *J. Mol. Liq.* 250 (2018) 26.
- [20] S. Li, B. Schmidt, Replica exchange MD simulations of two-dimensional water in graphene nanocapillaries: rhombic versus square structures, proton ordering, and phase transitions, *Phys. Chem. Chem. Phys.* 21 (2019) 17640.
- [21] J. Dix, L. Lue, P. Carbone, Why different water models predict different structures under 2D confinement, *J. Comput. Chem.* 39 (2018) 2051.
- [22] M. Neek-Amal, F.M. Peeters, I.V. Grigorieva, A.K. Geim, Commensurability effects in viscosity of nanoconfined water, *ACS Nano* 10 (2016) 3685.
- [23] G. Cicero, J.C. Grossman, E. Schwegler, F. Gygi, G. Galli, Water confined in nanotubes and between graphene sheets: A first principle study, *J. Am. Chem. Soc.* 130 (2008) 1871.
- [24] S.A. Deshmukh, G. Kamath, G.A. Baker, A.V. Sumant, S.K.R.S. Sankaranarayanan, The interfacial dynamics of water sandwiched between graphene sheets are governed by the slit width, *Surf. Sci.* 609 (2013) 129.
- [25] S. Ruiz-Barragan, F. Sebastiani, P. Schienbein, J. Abraham, G. Schwaab, R.R. Nair, M. Havenith, D. Marx, Nanoconfinement effects on water in narrow graphene-based slit pores as revealed by THz spectroscopy, *Phys. Chem. Chem. Phys.* 24 (2022) 24734.
- [26] Y. Yu, C. Yang, M. Baggio, A.E. Phillips, A. Zaccione, L. Zhang, R. Kajimoto, M. Nakamura, D. Yu, L. Hong, The  $\omega^3$  scaling of the vibrational density of states in quasi-2D nanoconfined solids, *Nat. Commun.* 13 (2022) 3649.
- [27] R.M. Stratt, The instantaneous normal modes of liquids, *Acc. Chem. Res.* 28 (1995) 201.
- [28] T. Keyes, Instantaneous normal mode approach to liquid state dynamics, *J. Phys. Chem. A* 101 (1997) 2921.
- [29] M. Cho, G.R. Fleming, S. Saito, I. Ohmine, R.M. Stratt, Instantaneous normal mode analysis of liquid water, *J. Chem. Phys.* 100 (1994) 6672.
- [30] S. Saito, I. Ohmine, Off-resonant fifth-order nonlinear response of water and CS2: Analysis based on normal modes, *J. Chem. Phys.* 108 (1998) 240.
- [31] S.L. Chang, T.M. Wu, C.Y. Mou, Instantaneous normal mode analysis of orientational motions in liquid water: Local structural effects, *J. Chem. Phys.* 121 (2004) 3605.
- [32] P.H. Tang, T.M. Wu, Instantaneous normal mode analysis for OKE reduced spectra of liquid and supercooled water: Contributions of low-density and high-density liquids, *J. Mol. Liq.* 301 (2020), 112363.
- [33] S. Plimpton, Fast parallel algorithms for short-range molecular dynamics, *J. Comput. Phys.* 117 (1995) 1.
- [34] J.L.F. Abascal, C. Vega, A general purpose model for the condensed phases of water: TIP4P/2005, *J. Chem. Phys.* 123 (23) (2005) 234505.
- [35] J.P. Hansen, I.R. McDonald, *Theory of Simple Liquids*, Academic Press, NY, 2006.
- [36] M.P. Allen, D.J. Tildesley, *Computer Simulation of Liquids*, Oxford University Press, NY, 1987.
- [37] S.A. Nosé, A unified formulation of the constant temperature molecular dynamics method, *J. Chem. Phys.* 81 (1984) 511.
- [38] W.G. Hoover, Canonical dynamics: equilibrium phase-space distributions, *Phys. Rev. A* 31 (1985) 1695.
- [39] P. Kumar, S.V. Buldyrev, F.W. Starr, N. Giovambattista, H.E. Stanley, Thermodynamics, structure, and dynamics of water confined between hydrophobic plates, *Phys. Rev. E* 72 (2005), 051503.
- [40] A. Lazar, D. Chandler, Hydrogen-bond kinetics in liquid water, *Nature* 379 (1996) 55.
- [41] S. Han, M.Y. Choi, P. Kumar, H.E. Stanley, Phase transitions in confined water nanofilms, *Nat. Phys.* 6 (2010) 685.
- [42] T. Kalbfleisch, T. Keyes, Untangling the physical contributions to instantaneous normal mode approximations: Inhomogeneous broadening, motional narrowing, and energy relaxation, *J. Chem. Phys.* 108 (1998) 7375.
- [43] G. E. Walrafen, in: *Water: Comprehensive Treatise*, edited by F. Franks, Plenum, New York, 1972, Chap. 1.
- [44] J. Martí, C. Calero, G. Franzese, Structure and dynamics of water at carbon-based interfaces, *Entropy* 19 (2017) 135.
- [45] T.M. Wu, W.J. Ma, S.F. Tsay, Potential effects on instantaneous normal modes of liquids, *Physica A* 254 (1998) 257.
- [46] H.E. Stanley, S.V. Buldyrev, N. Giovambattista, E.L. Nave, S. Mossa, A. Scala, F. Sciortino, F.W. Starr, M. Yamada, Application of statistical physics to understand static and dynamic anomalies in liquid water, *J. Stat. Phys.* 110 (2003) 1039.
- [47] S.D. Bembeneck, B.B. Laird, Instantaneous normal modes and the glass transition, *Phys. Rev. Lett.* 74 (1995) 936.
- [48] A. Zaccione, M. Baggio, Universal law for the vibrational density of states of liquids, *Proc. Natl. Acad. Sci. USA* 118 (2021), e2022303118.
- [49] C. Stamper, D. Cortie, Z. Yue, X. Wang, D. Yu, Experimental confirmation of the universal law for the vibrational density of states of liquids, *J. Phys. Chem. Lett.* 13 (2022) 3105.
- [50] K.H. Tsai, T.-M. Wu, Local structural effects on low-frequency vibrational spectrum of liquid water: The instantaneous-normal-mode analysis, *Chem. Phys. Lett.* 417 (4–6) (2006) 389–394.